

INTERNAL PRESSURE – STRESSING AND FORMING*

I. DOLTSINIS

Faculty of Aerospace Engineering and Geodesy, University of Stuttgart, Stuttgart, Germany.

ABSTRACT

Internal pressure as a loading mode concerns numerous engineering applications and technological processes. The present account deals with the material, the continuum, and the structural level. In addition to the stressing aspect, internal pressure is considered as the driving force in certain metal forming operations. The presentation of the subject bases on established solutions, less known results and technological applications.

Keywords: containers, forming operations, porous solids, shells.

1 INTRODUCTION

Internal pressure, caused by contained gaseous or liquid substances, is of interest on the material level as well as for engineering structures and components. Porous materials are considered with regard to the effect of pressure in the pores on the constitutive description. The finite element formalism is conveniently adapted to the action of pressure in the porous material. Investigations within the material structure suggest reference to the stress distribution around pressurized pores. In this context, analytical solutions available in the literature have been interpreted for cavities of various shapes in the elastic plane. Stress intensity factors for cracks emanating from elliptical holes enter the numerical simulation of microfracturing processes in porous brittle materials. A pronounced dependence on the structural pattern necessitates statistical considerations with respect to the strength.

Regarding engineering structures and structural elements, analytical approaches are known for the hollow cylinder and the sphere in elasticity and plasticity. Shell structures serve frequently as liquid tanks, pressure vessels, inflated membranes and the like. The subject is surveyed from the point of view of membrane theory and the possibilities of failure are briefly discussed. Numerical analysis by computer algorithms is not restricted to the membrane assumption. Depending on the case, adequate representation of the problem may require employment of shell- or bulk solid finite elements.

Apart from containment, internal pressure performs the task of formgiving and formkeeping of shell-like structures and components. Both issues are of technological importance. Formkeeping is of concern to inflated membranes. Pneumatic shaping has been applied, as a concept, to the construction of roofs by plastic deformation of thin metallic sheets at ambient temperature. The manufacturing process of superplastic forming, on the other hand, is effected by gas pressure on metallic blanks at elevated temperature. Of interest, the optimization of the process by controlling the forming pressure, and net-shape forming. The development of dedicated finite element methodology has been considerably promoted by industrial aerospace engineering.

2 POROUS MATERIAL

2.1 Continuum approach

In an elastic solid with homogeneously distributed microscopic porosity the stress σ is controlled by both the strain ε and the internal pressure p in the pores:

$$\boldsymbol{\sigma} = \kappa \boldsymbol{\varepsilon} - a_p p \boldsymbol{e}. \quad (1)$$

The matrix κ comprises the elasticity coefficients. The pressure carries part of the normal stresses, the vector $\boldsymbol{e} = \{1 \ 1 \ 1 \ 0 \ 0 \ 0\}$ effects the proper allocation. The factor a_p is considered a material parameter [1].

From a micromechanics perspective the macroscopic, virtually homogeneous stress σ and strain ε are obtained as the averages of the fields in the elementary volume V , Fig. 1:

$$\boldsymbol{\sigma} = \frac{1}{V} \int_{V_m} \boldsymbol{\sigma}_m dV - \chi p \boldsymbol{e}, \quad \boldsymbol{\varepsilon} = \frac{1}{V} \int_{V_m} \boldsymbol{\varepsilon}_m dV + \boldsymbol{\varepsilon}_p. \quad (2)$$

The stress $\boldsymbol{\sigma}_m$ varies within the part V_m occupied by the solid material as does the strain $\boldsymbol{\varepsilon}_m$. The porosity $\chi = (V - V_m)/V$ defines the volume fraction subjected to the pressure p . In the macroscopic strain the constituent $\boldsymbol{\varepsilon}_p$ accounts for the displacements along the pore boundaries. With $\boldsymbol{\sigma}_m = \kappa_m \boldsymbol{\varepsilon}_m$ for the elastic solid phase, eqn (2) gives

$$\boldsymbol{\sigma} + \chi p \boldsymbol{e} = \kappa_m (\boldsymbol{\varepsilon} - \boldsymbol{\varepsilon}_p) = \kappa \boldsymbol{\varepsilon} - \kappa_m (\boldsymbol{\varepsilon}_p - \boldsymbol{\varepsilon}_0). \quad (3)$$

For an interpretation of the macroscopic relation in eqn (1), it has been observed that in the absence of pressure the first equality becomes $\boldsymbol{\sigma} = \kappa_m (\boldsymbol{\varepsilon} - \boldsymbol{\varepsilon}_0) = \kappa \boldsymbol{\varepsilon}$, used in obtaining the second equality. The contribution of empty pores ($p = 0$) to the strain is denoted $\boldsymbol{\varepsilon}_0$, the elastic material stiffness matrix κ appertains to the overall behavior of the porous material, no pressure. The corrective term $\kappa_m (\boldsymbol{\varepsilon}_p - \boldsymbol{\varepsilon}_0)$ has been incorporated in eqn (1) by the empirical factor a_p which modifies the pressure term to $a_p p \neq \chi p$.

2.2 Ceramic rod with multiple channels

The rod of circular cross-section with interior channels in Fig. 2 (1 m in length, 0.020 m in diameter) is of macroporous ceramic. It serves in filtration equipments whereby the channels are subjected to fluid pressure.

The load carrying capacity of the part is determined by the stress distribution in conjunction with the strength of the brittle material. The highest principal stress σ_v , considered decisive for rupture, is plotted in Fig. 2 as a result of elastic finite element analysis for plane strain conditions. The overpressure by the medium in the channels is imposed on the inner surfaces. It is degraded through the porous ceramic to the ambient value at the outer surface.

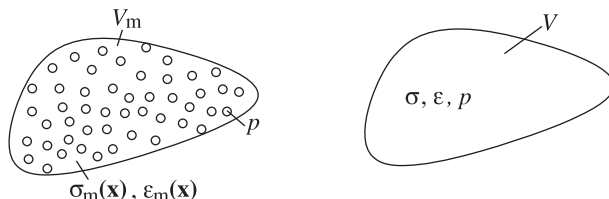


Figure 1: Solid with pressurized pores and equivalent homogeneous material.

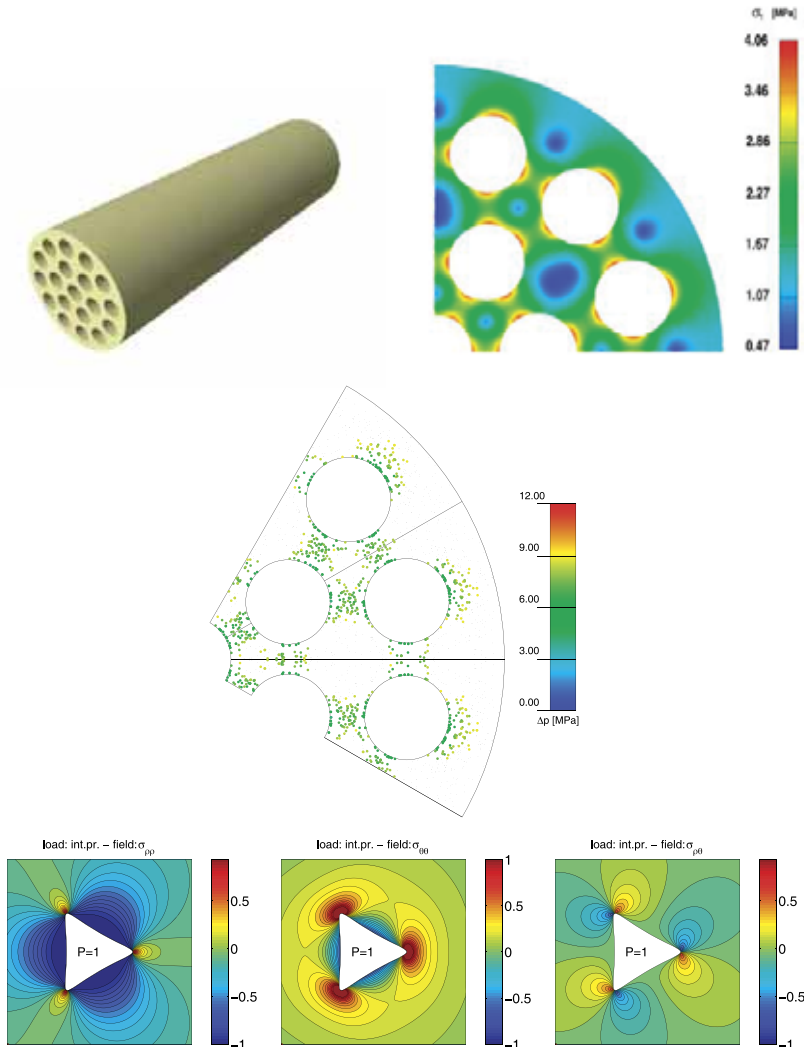


Figure 2: Ceramic filter support. Distribution of principal stress σ_1 in plane strain for $\Delta p = 5.0$ MPa between channels and outer surface. Frequency of critical locations. Below: Stress distribution around triangular pore at unit pressure (radial-, circumferential- and shear component). The analytical solution is deduced from Savin [8], the presentation refers to adjusted curvilinear ρ , θ -coordinates [4].

With reference to eqn (1) for the local stress, the pressure in the material gives rise to loads at the interior mesh nodal points as for initial stresses.

The material strength varies randomly within the part. Laboratory tests support the description by Weibull statistics [2]. Sampling at random the strength distribution in the finite element model and comparing with the computed stress field determines the frequency of locations prone to rupture at each level of channel pressure. Results from 1.000 realizations

of the strength distribution reveal that most critical to incipient failure are the vicinity of the pressurized channels and the ligaments, the locations of stress concentration. It becomes evident that the stress distribution overwhelms the scatter in material strength. Reliability assessment requires further investigations [3].

2.3 Fracturing of porous microstructure

Tasks related to the strength of materials may require investigation of the stress field around pressurized cavities below and above the continuum level. Stress concentrations because of holes in the elastic plane (Fig. 2) have been studied analytically in [4] for various simple shapes by the method of complex stress functions due to Kolosov [5] and Muskhelishvili [6]; see also Stevenson [7] and Savin [8].

Figure 3 displays the fracture pattern obtain numerically for an artificial material structure exposed to internal pressure in the pores. The pore pressure gives rise to the nucleation of cracks assumed propagating along grain boundaries. A grain interface of length L is considered to form a crack if

$$\int_L G dl = \int_L \frac{K^2}{E} dl \geq 2\gamma_s L \quad (4)$$

The energy release rate G of the elastic solid is related to the stress intensity factor K , which accompanies the singularity at the crack tip, by the elastic modulus E appertaining to either plane stress or plane strain. The specific surface energy of the material is denoted as γ_s . Of particular interest in the present context is the straight crack in the elongation of the semi-axis of an elliptical hole, Fig. 3. For internal pore pressure p the solution of Berezhnitskii [9] gives the stress intensity factor by the expression

$$\left(\frac{K}{\pi p} \right)^2 = \left(a + \frac{1}{2} \right) \frac{(1+l/a)^3 - 1}{(1+l/a)^2 - m} \frac{(1+l/a) + 1}{(1+l/a) + m}, \quad m = \frac{a-b}{a+b}. \quad (5)$$

The algorithm simulating fracturing in artificial material structures exposed to internal pore pressure has been based on suitable modifications of the above result [4]. Fluctuations in the microstructure suggest statistical considerations regarding the strength [2].

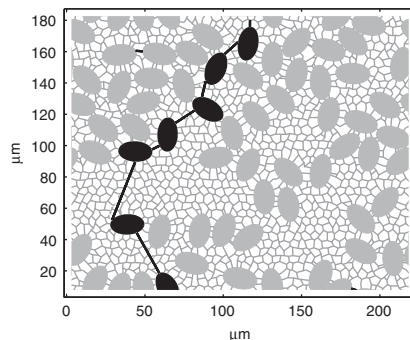
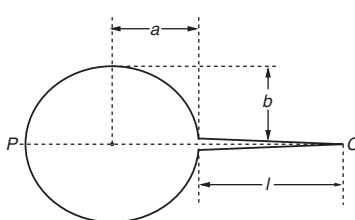


Figure 3: Study on fracture for plane microstructure due to pressure in pores of elliptical shape.

3 SHELLS UNDER INTERNAL PRESSURE

3.1 Elementary considerations

The subject is of importance for liquid tanks, pressure vessels, inflated membranes and similar. Shells are represented by the middle surface and a possibly varying thickness s . The analysis simplifies for thin-walled shells when bending is neglected. Then, variations of the stress across the thickness are discarded; the stress state results to membrane forces defined as normal- and shear flow transmitted per unit length. Rotational symmetry of shell geometry and loading excludes shear and reduces the membrane forces to the meridional component N_ϕ and the circumferential N_θ along parallel circles (Fig. 4). In the present context the loading is considered distributed over the surface with two components: p_ϕ and p_n . The statement of equilibrium for the shell element normal to the middle surface gives

$$\frac{N_\phi}{R_1} + \frac{N_\theta}{R_2} = p_n. \quad (6)$$

The radius of curvature R_1 is in the meridian plane, R_2 equals the distance of the middle surface to the axis of revolution along the normal. It is noted that eqn (6) is not restricted to rotational symmetry, but applies to every shell geometry provided that the ϕ, θ -system follows the lines of principal curvature of the surface. Equation (6) relates the circumferential force N_θ and the meridional force N_ϕ . The meridional force is obtained by considering the equilibrium of a portion of the shell above a parallel circle. Loading by internal pressure ($p_\phi = 0, p_n = p$) results to

$$N_\phi = \frac{pr}{2 \sin\phi} = \frac{pR_2}{2}; \quad N_\theta = pR_2 \left(1 - \frac{R_2}{2R_1}\right). \quad (7)$$

For a shell shaped as an ellipsoid of revolution with semi-axes a and b (Fig. 4) the forces at the pole ($R_1 = R_2 = a^2/b$), and at the equator ($R_1 = b^2/a, R_2 = a$) are

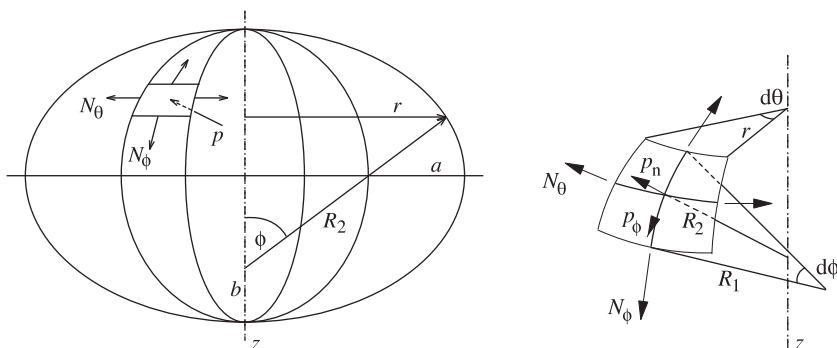


Figure 4: Shell of revolution. Shell element under axisymmetric conditions.

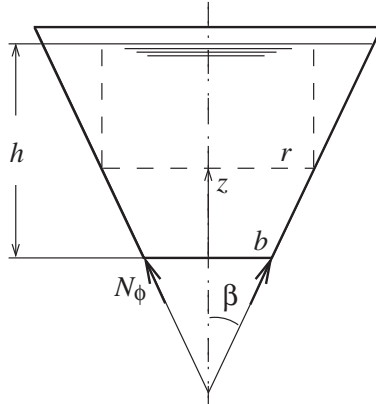


Figure 5: Conical liquid tank.

$$N_\phi = N_\theta = \frac{pa^2}{2b}, \quad N_\phi = \frac{pa}{2}, \quad N_\theta = pa \left(1 - \frac{a^2}{2b^2}\right). \quad (8)$$

The meridional force N_ϕ is positive, but the circumferential force N_θ becomes negative at the equator if the ellipsoid is flat such that $a/b > \sqrt{2}$.

Other pressurized containers with simple geometry are treated analogously. More general analytical solutions are sought in terms of a stress function. Several examples are given in the classical book by Flügge [10]. Membrane strains are determined from the stresses by the applicable constitutive law of the material. If the displacements turn out to be finite the equilibrium condition must be stated for the updated configuration of the shell.

Shells are prone to buckling instability where compressive stresses appear. An example is the conical tank shown in Fig. 5. The tank (conus angle β), supported at the lower edge (radius b), is filled up to the height h with liquid of specific weight γ , the weight of the tank wall is assumed negligible. The fluid induces compressive forces N_ϕ along meridians and tensile forces N_θ along the periphery:

$$N_\phi = -\gamma(h-z)^2 \left(1 + \frac{h-z}{3r} \tan \beta\right) \frac{\tan \beta}{2 \cos \beta}, \quad N_\theta = pR_2 = \gamma \frac{(h-z)r}{\cos \beta}. \quad (9)$$

The compressive meridional force in eqn (9) is seen to become quickly higher towards the bottom of the tank ($z = 0$). An increasing level h of the liquid may cause buckling of the bottom part and catastrophic collapse of the tank. The tensile nature of the circumferential membrane force, eqn (9), has a stabilizing effect with respect to the buckling, but may favour other variants of failure like by plastic yielding and fracture.

3.2 Heating-up of liquid zinc tank

The heating phase of liquid zinc containers may become critical to cracking by stress corrosion. The tank shown in Fig. 6 with a capacity of 140 tons stands on a grid of concrete beams. Melting of the zinc is by four burners at the upper third of the side walls. Bulging of the side walls during melting is prevented by the three horizontal supports S1, S2, S3.

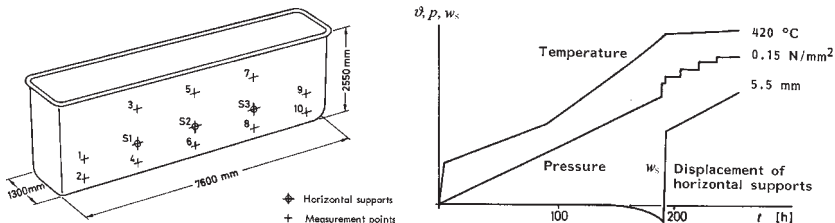


Figure 6: Tank for liquid zinc. Geometry and measurement points (left). Schematic variation of heating-up temperature ϑ , pressure p , displacement of horizontal supports w_s (right).

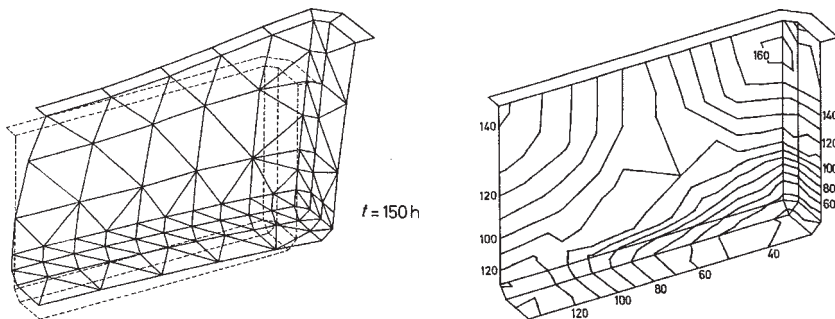


Figure 7: Deformation of tank (40 \times magnified). Principal stress σ_1 on inside [N/mm²].

The elastoplastic analysis by finite elements [11] takes advantage of the double symmetry of the problem. The loading is by the temperature variation, the pressure from the melting zinc and the registered displacement of the horizontal supports. The pressure from the melting zinc conforms to the development of the temperature. Initially, the tank is filled with 100 tons of zinc, assumed melted after 190 hours. In the sequence 40 tons are added gradually.

The temperature interval in question alters the properties of the steel material in elasticity and plasticity. Results of the computer simulation of the heating process of the tank (255 h) are displayed in Fig. 7 for an instant of interest. During the first 50 hours the deformation of the tank alters the support conditions such that only the front end regions remain in contact with the ground. The principal stress σ_1 refers to the inner surface of the tank which is prone to stress corrosion cracking. Maximum stresses appear after 150 hours near the rim stiffener on the top of the tank and at the transition between side walls and bottom. The shear stress in the walls is negligible.

4 FORMGIVING AND FORMKEEPING

4.1 Pneumatic shaping

Space structures consisting of soft elements, like cable networks and textile membranes, must be prestressed while assembled in order to become stiff. On the contrary, space

structures formed by plastic deformation of sheet metal become stiff in the formgiving phase; maintenance of prestress is not required.

A particular technique is bulging of thin sheet material at room temperature via pneumatic pressure [12]. The construction specified in Fig. 8 consists of two circular sheets (0.3 mm steel) preformed to slightly curved caps and joined hermetically at a peripheral ring frame. Bulging induces plastic deformation in the metallic sheets; removal of the pressure leaves a stiff configuration. Formgiving is actually by quasistatic inflation up to pressure $p = 29.43$ kPa. The interest of a computer simulation by finite elements [13] lies in a rapid application and removal of the forming pressure to twice the static value as a cosine pulse of 20 ms duration. The induced dynamic effect is predicted to reduce the sheet thickness at the apex from 0.3 mm to 0.1995 mm. Figure 9 traces the history of dynamic deformation of the spherical sheet cap to a paraboloidal dome. The isometric plot of the deforming geometry shows an initial phase of permanent deformation followed by elastic oscillations about the new configuration.

Figure 10 refers to the small scale laboratory model of a membrane deformed permanently to a cushion by pneumatic pressure. The aluminum sheets (upper and lower, thickness: 0.03 mm) are stiffened along the axes of plane symmetry and along the diagonals by strips

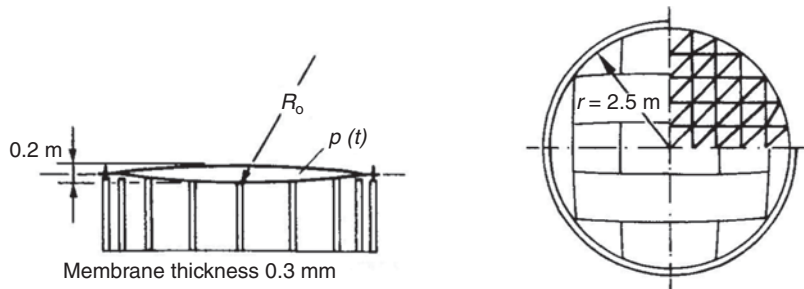


Figure 8: Metallic roof model formed by inflation pressure.

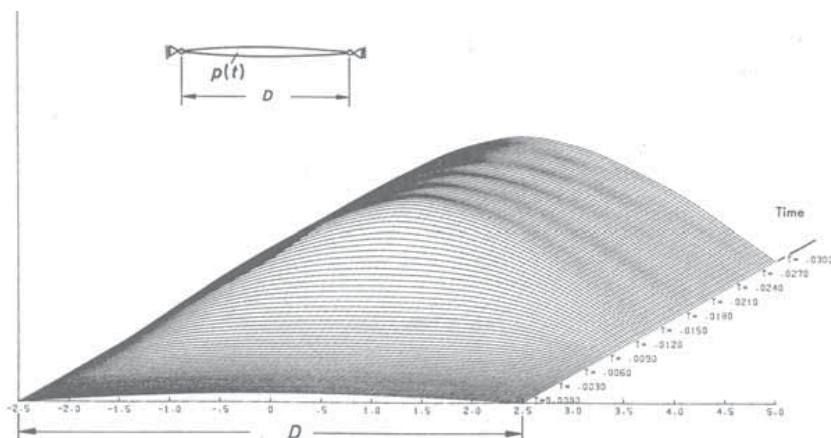


Figure 9: History of dynamic dome forming.

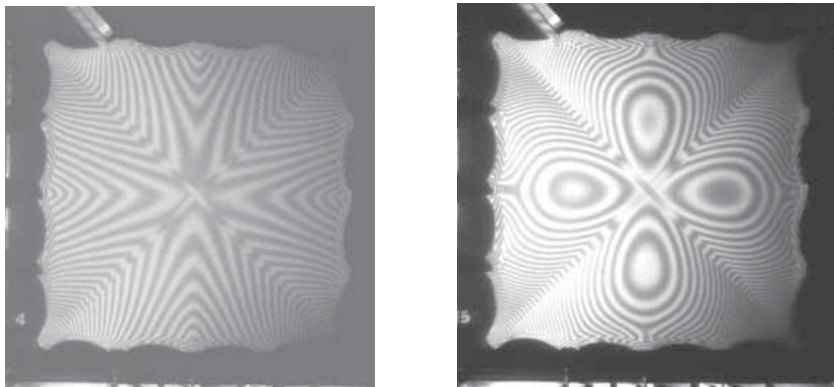


Figure 10: Membrane model. Prior to inflation (left), after forming (right).

(cross-section: 3.38 mm^2). Figure 10 gives an impression of the initial and the final shape of the model considered from above. The Moiré image in the left frame refers to the state when pressure is not yet applied ($p = 0$), upper and lower sheet are in touch; referring to a roof structure, the experimental model is fixed such that curvatures arise. The right frame visualizes the final shape of the upper sheet at maximum inflation pressure $p = 2639 \text{ Pa}$.

4.2 Superplastic forming

The term superplasticity denotes a deformation process that produces large permanent elongations in metallic materials subjected to tension. This advantage of certain materials is utilized for manufacturing in a single cycle structural parts that require high permanent deformation. Essential to superplasticity are specific thermal and mechanical conditions which accentuate the dependence of the flow stress σ on the deformation rate δ such that local necking is prohibited. Modeling is as for an isochoric viscous material with zero yield limit. The flow stress depends also on the grain size d which changes following the grain growth kinetics of the material:

$$\sigma = f(\delta, d). \quad (10)$$

Superplastic deformation is a slow process which requires the maintenance of high temperature for a longer period. In industrial practice sheets or plates of the metal are bulged under the action of gas pressure to form shell-like structural parts. Figure 11 refers to a conical structural component (335 mm in height) manufactured by bulging a pre-contoured thick circular plate (32–18.5 mm, 400 mm diameter). The superplastic forming process requires 13 hours whereby Ti-6Al-4V titanium alloy at the temperature of 1200 K is deformed under pressure imposed as prescribed by the industrial manufacturer: the intensity, increasing from zero, attains the final value of 1.4 N/mm^2 within 4 hours. The study has been one of the first pertaining to industrial practice in aerospace engineering [14].

The inner surface of the component is subjected to the gas pressure. The outer surface progressively comes into contact with the die and slides along the wall. In practice sliding friction is avoided; its effect is of interest when conceiving the process. Friction was found to slow down the forming operation to 20 hours and alters the thickness distribution in the product, introducing extensive thinning at the apex.

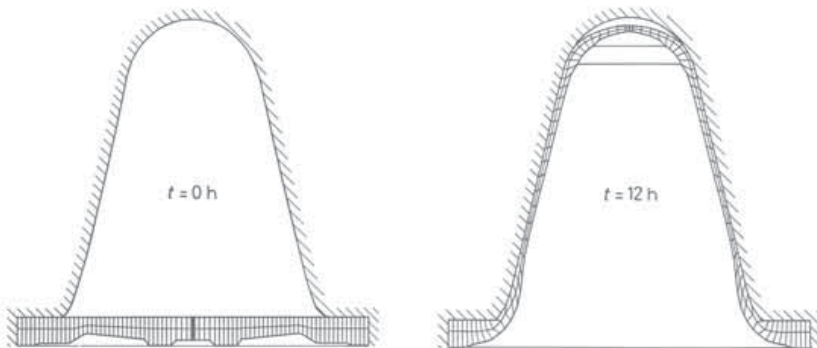


Figure 11: Conical aerospace component.

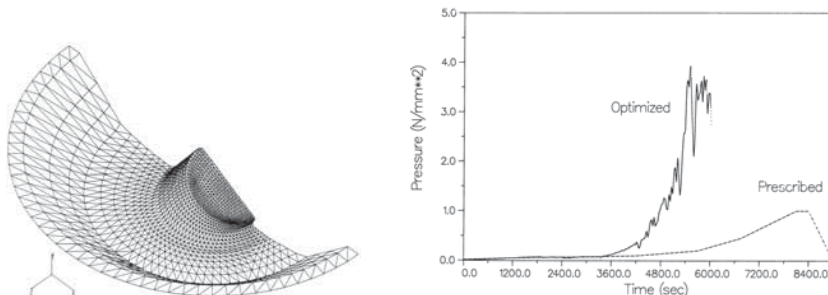


Figure 12: Part formed by superplastic bulging of flat sheet; optimized gas pressure.

The control of the forming pressure is of great importance for both, maintaining superplastic conditions and efficiency of manufacturing. The gas pressure is controlled such that the maximum equivalent rate of deformation in the part meets with an optimum value favourable for superplasticity. It is demonstrated in Fig. 12 (symmetric half formed of 1.8 mm circular titanium sheet, 250 mm diameter) that a pressure history prescribed by engineering experience and intuition may prove insufficient at least with regard to efficiency. Improved process design is obtained when optimizing the forming pressure in conjunction with numerical computer simulation.

In net-shape forming a requested geometry of the product is achieved as an immediate result of the single process, with no additional operations. The task to be performed in the design phase of the process is to specify the initial geometry of the work-piece material such that the deformation produces the desired configuration. This inverse problem of pre-contouring the blank has been treated successfully for the industrial production of a hemispherical satellite tank. Computer simulation of superplastic forming is detailed in [15].

REFERENCES

- [1] Biot, M.A., General theory of three-dimensional consolidation. *Journal of Applied Physics*, **12**, pp. 155–164, 1941. [doi: http://dx.doi.org/10.1063/1.1712886](http://dx.doi.org/10.1063/1.1712886)
- [2] Doltsinis, I. & Osterstock, F., Modelling and experimentation on the strength of porous ceramics. *Archives of Computational Methods in Engineering*, **12**, pp. 303–336, 2005. [doi: http://dx.doi.org/10.1007/BF02736178](http://dx.doi.org/10.1007/BF02736178)

- [3] Doltsinis, I., *Stochastic Methods in Engineering*, WIT Press: Southampton, Boston, 2012.
- [4] Doltsinis, I. & Dattke, R., Modelling the damage of porous ceramics under internal pressure. *Computer Methods in Applied Mechanics and Engineering*, **199**, pp. 29–46, 2001. [doi: *http://dx.doi.org/10.1016/S0045-7825\(01\)00243-2*](http://dx.doi.org/10.1016/S0045-7825(01)00243-2)
- [5] Kolosov, G.V., *On the Application of Complex Function Theory to a Plane Problem of the Mathematical Theory of Elasticity*, (Orig. Russian), Doctoral Thesis, University of Yuriew, Yuriew Publ. Co., 1909.
- [6] Muskhelishvili, N.I., *Some Basic Problems of the Mathematical Theory of Elasticity*, Noordhoff: Groningen, 1953.
- [7] Stevenson, A.C., Complex potentials in two-dimensional elasticity. *Proc. R. Soc. A*, **184**, pp. 129–179, 1945.
- [8] Savin, G.N., *Stress Concentration Around Holes*, Pergamon Press: Oxford, 1961.
- [9] Berezhnitskii, L.T., Propagation of cracks terminating at the edge of a curvilinear hole in a plate. *Soviet Materials Science*, **2**, pp. 12–23, 1966.
- [10] Flügge, W., *Stresses in Shells*, Springer: Berlin, 1960. [doi: *http://dx.doi.org/10.1007/978-3-662-01028-0*](http://dx.doi.org/10.1007/978-3-662-01028-0)
- [11] Doltsinis, I., *Elements of Plasticity - Theory and Computation*, WIT Press: Southampton, Boston, 2000. 2nd edn., 2010.
- [12] Greiner, S., *Membrantragwerke aus dünnem Blech*, Werner-Verlag: Düsseldorf, 1983.
- [13] Argyris, J., Doltsinis, I. & Willam, K., New developments in the inelastic analysis of quasistatic and dynamic problems. *International Journal for Numerical Methods in Engineering*, **14**, pp. 1813–1850, 1979. [doi: *http://dx.doi.org/10.1002/nme.1620141206*](http://dx.doi.org/10.1002/nme.1620141206)
- [14] Argyris, J. & Doltsinis, I., A primer on superplasticity in natural formulation. *Computer Methods in Applied Mechanics and Engineering*, **46**, pp. 83–131, 1984. [doi: *http://dx.doi.org/10.1016/0045-7825\(84\)90130-0*](http://dx.doi.org/10.1016/0045-7825(84)90130-0)
- [15] Doltsinis, I., *Large Deformation Processes of Solids - From Fundamentals to Numerical Simulation and Engineering Applications*, WIT Press: Southampton, Boston, 2004.

* Keynote address: HPSM 2012, 6th International Conference on High Performance Structures and Materials, 19–21 June 2012, New Forest, UK.